JOURNAL OF AIRCRAFT
Vol. 38, No. 6, November–December 2001

Multidisciplinary Design Optimization of a Transonic Commercial Transport with Strut-Braced Wing

Frank H. Gern,* Andy Ko,† Erwin Sulaeman,† John F. Gundlach,† and Rakesh K. Kapania‡
Virginia Polytechnic Institute and State University, Blacksburg, Virginia 24061-0203
and
Raphael T. Haftka§
University of Florida, Gainesville, Florida 32611-6250

The multidisciplinary design optimization of a strut-braced wing (SBW) aircraft and its benefits relative to a conventional cantilever wing configuration are presented. The multidisciplinary design team is divided into aerodynamics, structures, aeroelasticity, and the synthesis of the various disciplines. The aerodynamic analysis uses simple models for induced drag, wave drag, parasite drag, and interference drag. The interference drag model is based on detailed computational fluid dynamics analyses of various wing–strut intersections. The wing structural weight is calculated using a newly developed wing bending material weight routine that accounts for the special nature of SBWs. The other components of the aircraft weight are calculated using a combination of NASA's flight optimization system and Lockheed Martin aeronautical systems formulas. The SBW and cantilever wing configurations are optimized using design optimization tools (DOT) software. Offline NASTRAN aeroelastic analysis results indicate that the flutter speed is higher than the design requirement. The minimum take-off gross weight SBW aircraft showed a 9.3% advantage over the corresponding cantilever aircraft design. The minimum fuel weight SBW aircraft showed a 12.2% fuel weight advantage over a similar cantilever aircraft design.

Introduction

VERY few recent transonic transport aircraft designs divert from a low cantilever wing with either wing or fuselage mounted engines. However, numerous alternative concepts have been introduced over the years to challenge the cantilever wing design paradigm. These include the joined wing, blended-wing–body, twin-fuselage and the strut-braced wing. This study exclusively compares the strut-braced wing concept (SBW) to the cantilever wing configuration.

Favorable interactions between structures, aerodynamics, and propulsion give the SBW potential for higher aerodynamic efficiency and lower weight than a cantilever wing. The strut provides bending load alleviation for the wing, allowing the wing thickness to be reduced for a given wing load. Reduced wing thickness decreases transonic wave drag and parasite drag, thus allowing the wing to unsweep for increased regions of natural laminar flow. Reduced overall weight, along with increased aerodynamic efficiency, permits engine size reduction.

As a result, significant performance gains over the cantilever wing are expected. A Multidisciplinary design optimization (MDO) approach is necessary to fully exploit the interdependencies of various design disciplines. Several SBW design studies have been conducted in the past,[1–6] although not with a full MDO approach until quite recently.[7–9]

The present study was enabled by NASA Langley Research Center with Lockheed Martin Aeronautical Systems (LMAS) as an industrial partner. The LMAS interactions added practical industry experience to the vehicle study. LMAS reviewed aspects of the Virginia Polytechnic Institute and State University design methods specific to the SBW.[9]

Several SBW concepts have been investigated within the project. Design studies cover wingtip engines, underwing engines, and fuselage-mounted engines with a T-tail. However, this paper highlights structural, aerodynamic, and aeroelastic aspects for fuselage-mounted engine SBW configurations.

Design Optimization

General Aspects

The Virginia Polytechnic Institute and State University SBW code models aerodynamics, structures, weights, performance, and stability and control of both cantilever and SBW configurations. Design optimization tools (DOT) software[10] optimizes the vehicles using the modified method of feasible directions. During a typical optimization run, between 15 and 22 design variables are used. These include several geometric variables such as wing span, chord lengths, thickness to chord ratios, strut geometry, and engine location, plus additional variables including engine maximum thrust and average cruising altitude. In addition, as many as 15 inequality constraints may be used (Table 1).

Each design variable is bound by two side constraints and is scaled to a value between 0 and 1 at the lower and upper limits, respectively. Different objective functions can be minimized during the optimization. Examples are takeoff gross weight (TOGW), economic mission TOGW weight, and fuel weight. The MDO code architecture is configured in a modular way, and the analysis consists of various subroutines representing the different design disciplines. The primary analysis modules include aerodynamics, wing bending material weight, total aircraft weight, stability and control, propulsion, flight performance, and field performance (Fig. 1).

Received 8 October 1999; revision received 7 July 2000; accepted for publication 23 March 2001.

*Research Associate, Multidisciplinary Analysis and Design Center for Advanced Vehicles, Department of Aerospace and Ocean Engineering; currently Research Assistant Professor, Center for Intelligent Material Systems and Structures, Virginia Polytechnic Institute and State University, Blacksburg, VA 24061-0261. Member AIAA.

†Graduate Research Assistant, Multidisciplinary Analysis and Design Center for Advanced Vehicles, Department of Aerospace and Ocean Engineering. Student Member AIAA.

‡Professor, Multidisciplinary Analysis and Design Center for Advanced Vehicles, Department of Aerospace and Ocean Engineering. Associate Fellow AIAA.

§Distinguished Professor, Department of Aerospace Engineering, Mechanics and Engineering Science. Fellow AIAA.

Mission Profile

The primary mission of interest is a 325-passenger, 7500-n mile range, Mach 0.85 transport aircraft with a 500-n mile fuel reserve (Fig. 2). Several technology groups distinguish the 1995 and 2010 technology level aircraft. Essentially, a 1995 technology aircraft represents an all-metallic benchmark similar to the Boeing 777, which also served as a validation example for the optimization. Projected aerodynamic improvements include drag reductions due to riblets on fuselage and nacelles, supercritical airfoils, active load management for induced drag reduction, and all movable control surfaces. Systems technologies include integrated modular flight controls, fly-by-light and power-by-light, simple high-lift devices, and advanced flight management systems. Airframe technologies allow weight savings from composite wing and tails and integrally stiffened fuselage skins. The propulsion technology is reflected in reduced specific fuel consumption.

Aerodynamics

Numerous iterations between both the Virginia Polytechnic Institute and State University SBW code and Lockheed's analysis software were made so that drag polars produced by each code are consistent at reference design conditions. The drag components considered in the Virginia Polytechnic Institute and State University SBW code are parasite drag, induced drag, interference drag, and wave drag. Unless specified otherwise, the drag model is identical to previous Virginia Polytechnic Institute and State University SBW studies.[8] A detailed description of the drag calculations can be found in Ref. 11.

Table 1 Optimization constraints

Constraint	Value
Aircraft zero fuel weight convergence	
Range Calculated	>Reference range
Initial cruise rate of climb	>500 ft/min
Maximum cruise section C_L	<0.7
Fuel weight	<Fuel capacity
C_N available	>C_N required
Wing tip deflection	<Maximum wing tip deflection at taxi bump condition
Second segment climb gradient	>2.4%
Balanced field length	<11,000 ft
Approach velocity	<140 kn
Missed approach climb gradient	>2.1%
Landing distance	<11,000 ft
Economic mission range calculated	>4000 n mile
Economic mission section $C_{L\,max}$	<0.7
Thrust at altitude	>Drag at altitude

Parasite Drag

To calculate the parasite drag, form factors are applied to the equivalent flat-plate skin-friction drag of all exposed surfaces on the aircraft. The amounts of laminar flow on the wing and tails are estimated by interpolating Reynolds number vs sweep data for F-14 and 757 glove experiments. Fuselage, nacelles, and pylon transition locations are estimated by an input transition Reynolds number. Laminar and turbulent flat-plate skin-friction form factors are calculated with LMAS formulas in the Virginia Polytechnic Institute and State University MDO code. LMAS form factors for wing, tails, fuselage, and nacelles are applied to the skin friction drag to obtain the parasite drag.

Induced Drag

The induced drag module uses a discrete vortex method to calculate the induced drag in the Trefftz plane.[8] Given an arbitrary, noncoplanar wing–truss configuration, it provides the optimum load distribution corresponding to the minimum induced drag. This load distribution is passed to the wing sizing subroutine. An additional lift-dependent parasite drag component was added to correlate with LMAS drag polars at off-design conditions.

Wave Drag

The wave drag is approximated with the Korn equation, modified to include sweep using simple sweep theory (see Refs. 7 and 8). This model estimates the drag divergence Mach number as a function of airfoil technology factor, thickness-to-chord ratio, section lift coefficient, and sweep angle. The airfoil technology factor was selected by Lockheed to agree with the LMAS wave drag. Finally, the wave drag coefficient of a wing strip is calculated from the critical Mach number. The total wave drag is found by integrating the wave drag of the strips along the wing.

Interference Drag

The benefits of a SBW configuration are reduced by a potential interference drag penalty at the junction of the strut with the fuselage

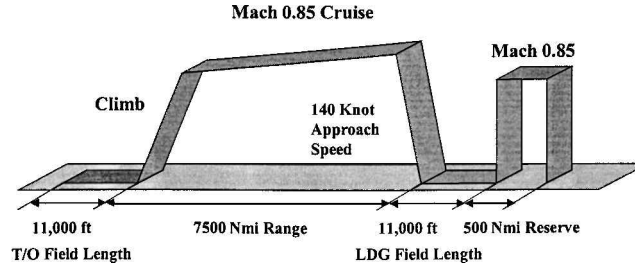

Fig. 2 Mission profile.

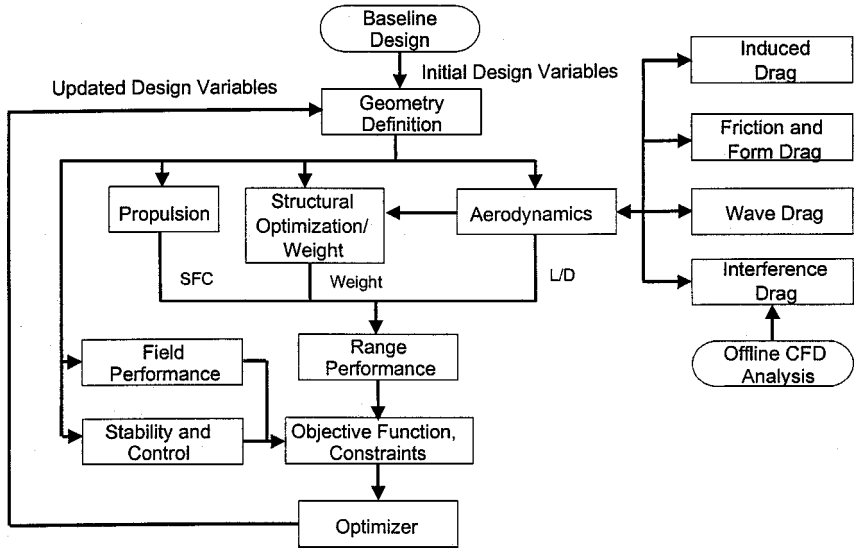

Fig. 1 Modular structure of the MDO process.

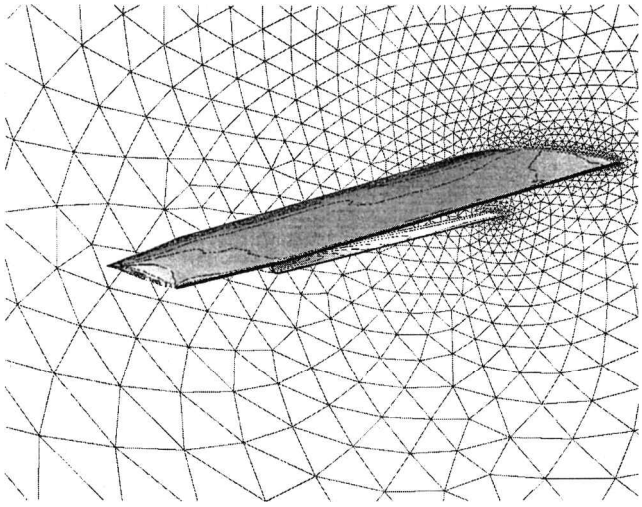

Fig. 3 CFD wing–strut interference drag analysis using unstructured grids.

and the wing. The interference drag between the wing–fuselage and strut–fuselage intersections is estimated using Hoerner equations based on subsonic wind-tunnel tests.[12]

The drag of wing–strut junctions in transonic flow can be significant due to the presence of shock waves and regions of separated flow. To alleviate the problem associated with a sharp wing–strut angle, the strut employed here is given the shape of an arch and intersects the wing perpendicularly. Analyses for an arch radius ranging from 1 to 4 ft were performed with computational fluid dynamics (CFD) tools (Fig. 3). Unstructured grids were obtained with the advancing-front methodology implemented in the code VGRIDns.[13,14] The Euler equations were solved using the CFD code USM3D[14,15] at the cruise Mach number of 0.85.

A convenient way to extract the interference drag penalty from a CFD calculation consists in subtracting the drag of the wing alone from the drag of the strut-braced wing design obtained with CFD. The resulting number is a ΔC_D penalty associated with the presence of the strut. As the arch radius is increased, the drag penalty decreases almost exponentially. From these results, a curve fit is produced and used in the present analysis to account for the drag of the wing–strut junction. The drag polars output from the Virginia Polytechnic Institute and State University MDO tool and LMAS modified NASA flight optimization system (FLOPS) agree within 1% on average for cantilever wing designs.[11]

Structures

Because of the unconventional nature of the proposed concept, commonly available weight calculation models for transport aircraft, such as the NASA Langley Research Center developed FLOPS,[16] are not accurate enough. Therefore, a special bending weight calculation procedure was developed, taking into account the influence of the strut on the structural wing design.

Load Cases

To determine the bending material weight of the SBW, two maneuver load conditions (2.5-g maneuver and -1.0-g pushover) and a taxi bump (-2.0 g) are considered to be design critical. For the -1.0-g pushover and for the -2.0-g taxi bump, the strut is not active, and the wing acts like a cantilever beam. Because the strut is not supporting the wing in these cases, very high deflections of the wing are expected for the -2.0-g taxi bump. As a result, an optimization procedure is implemented to distribute the bending material to prevent wing ground strikes. To maximize the beneficial influence of the strut on the wing structure, strut force and spanwise position of the wing–strut intersection are optimized by the MDO code for the 2.5-g maneuver load case. To attain acceptable aerodynamic characteristics of the strut, an airfoil cross section is considered. However, the strut is assumed to be designed in such way that it will not carry aerodynamic loads during cruise.

Structural Assumptions

Preliminary studies have shown buckling of the strut under the -1.0-g load condition to be the critical structural design requirement in single-strut configurations, resulting in high strut weights.[8] To address this issue, an innovative design strategy employs a telescoping sleeve/damper mechanism to allow the strut to be inactive during negative gravity maneuvers and active during positive gravity maneuvers. Thus, under the -1.0-g case, the wing acts like a cantilever beam. For positive gravity maneuvers, the wing can be analyzed as a strut-braced beam.

An even higher wing weight reduction can be obtained by optimizing the strut force and wing–strut junction location. On a typical optimum single-strut design, this means that the strut would first engage in tension at a certain positive load factor. This can be achieved by a slack in the wing–strut mechanism. The optimum strut force at 2.5 g is different from the strut force that would be obtained at 2.5 g if the strut were engaged for all positive values of the load factor. Therefore, the slack load factor is defined as the load factor at which the strut engages for the first time. It is important to have a positive slack load factor, otherwise the strut would be preloaded at the jig shape to achieve the optimum strut force.

Vertical Strut Offset

As mentioned earlier, an arch-shaped strut attachment is used to reduce the aerodynamic interference drag at the wing–strut junction. Nonlinear structural effects due to the arch strut attachment are considered to be of secondary order and beyond the accuracy of the present analysis. Therefore, in the structural modeling, the wing–strut junction is idealized as a vertical strut offset, connecting to a straight strut (Fig. 4) (Ref. 17). This allows a simplified analysis and sizing of the wing–strut junction without a significant loss in accuracy as compared to the full analysis of an arch-shaped wing–strut junction.

The vertical offset member is designed for a combined bending/tension loading. In this context, the horizontal component of the strut force is of special concern (Fig. 4). Because this horizontal force results in a considerable bending load on the offset piece, its weight increases dramatically with increasing strut force and offset length.

Consequently, it is imperative to employ MDO tools to obtain optimum values for vertical offset, strut force, and spanwise wing–strut breakpoint. This allows to tradeoff the two contrary design requirements: 1) a reduced offset length to reduce strut loading and 2) an increased offset length to reduce the wing–strut interference drag. After a complete design optimization with the vertical strut offset as an active design variable, the influence of the offset weight on the total strut weight becomes comparably small. For the wing bending weight and especially for the TOGW, it is almost immaterial.

Figure 5 shows the wing bending moment distributions for the design critical load cases of the fuselage-mounted engine SBW design. Because of the vertical strut offset, an additional bending moment is

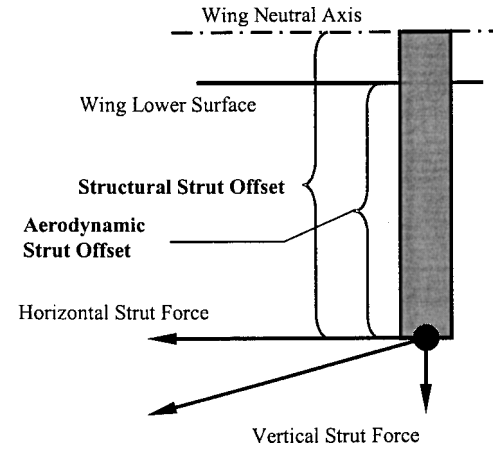

Fig. 4 Vertical strut offset and applied loads.

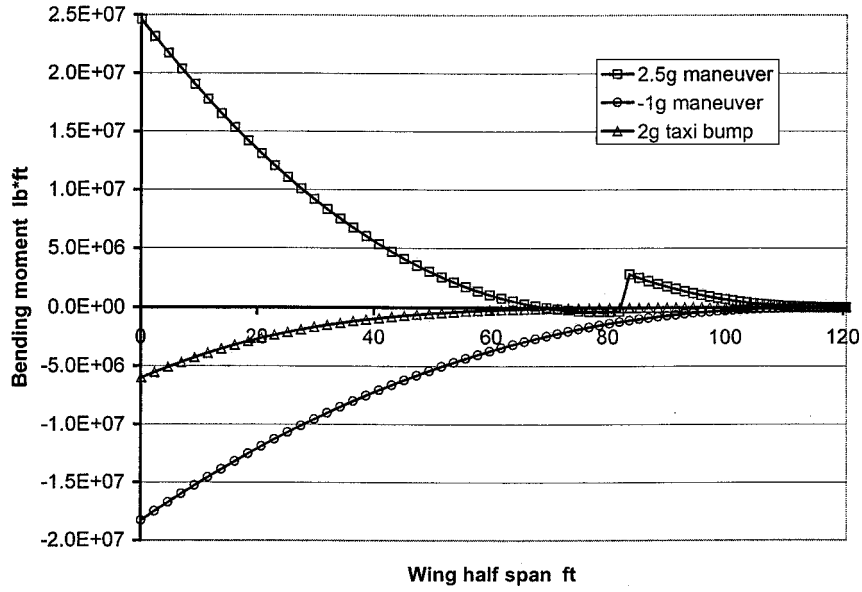

Fig. 5 Bending moment distributions for the design critical load cases of the fuselage-mounted engine SBW.

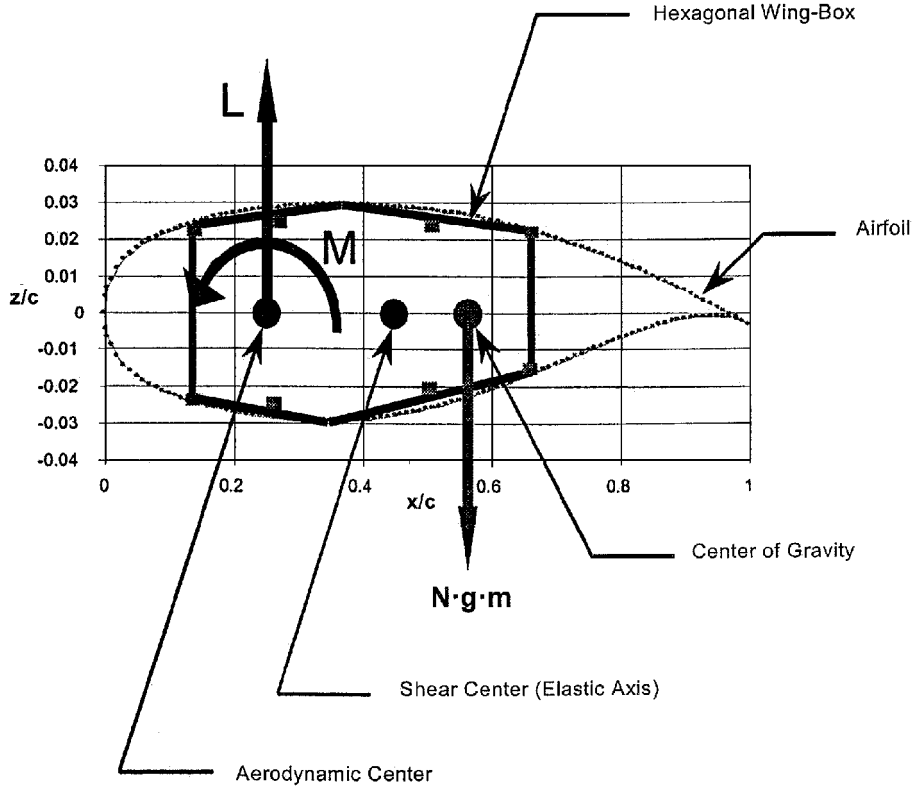

Fig. 6 Hexagonal wing–box and applied sectional forces and moments.

created at the wing–strut junction, leading to a discontinuity in the bending moment distribution. Because the strut is inactive in compression, the bending moment distributions for the −1.0-*g* pushover and for the 2.0-*g* taxi bump do not show this discontinuity.

Aeroelasticity

Hexagonal Wing–Box Model

A hexagonal wing–box model provided by LMAS was implemented into the code to provide accurate estimates of the wing–box torsional stiffness. This torsional stiffness becomes essential when calculating wing twist and flexible wing spanload, as well as for the incorporation of aeroelastic constraints and design variables into the MDO optimization (Fig. 6). A detailed description of the hexagonal wing–box model and the flexible wing sizing procedure can be found in Ref. 17. Based on Lockheed Martin's experience in wing sizing, the wing–box geometry varies in the spanwise direction, with optimized area and thickness ratios for spar webs, spar caps, stringers, and skins. Furthermore, minimum gauges and maximum stress cutoffs can be accurately applied.

Aeroelasticity

Beyond rendering accurate quantities for bending and torsional stiffness, the hexagonal wing–box was used to create input data and realistic sizing for detailed finite element analyses. With these data, a detailed finite element model of the structural wing–box is computed and analyzed using NASTRAN. It consists of 630 grid points, 1239 rod elements, and 3232 plate elements (Fig. 7). The

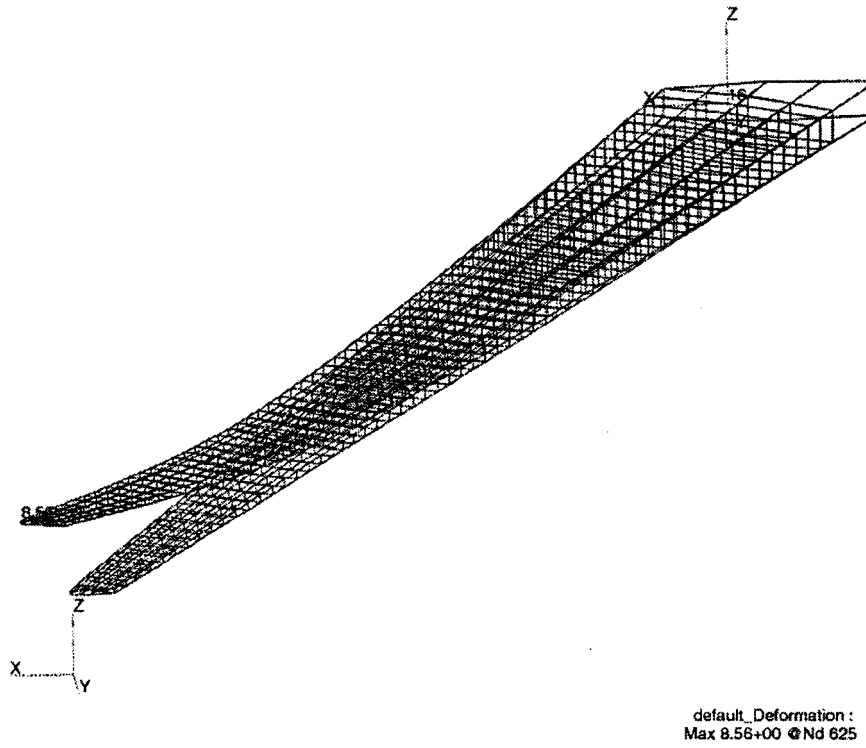

Fig. 7 NASTRAN finite element model of the hexagonal wing–box; deformation of the wing–box during a 2.5-*g* maneuver.

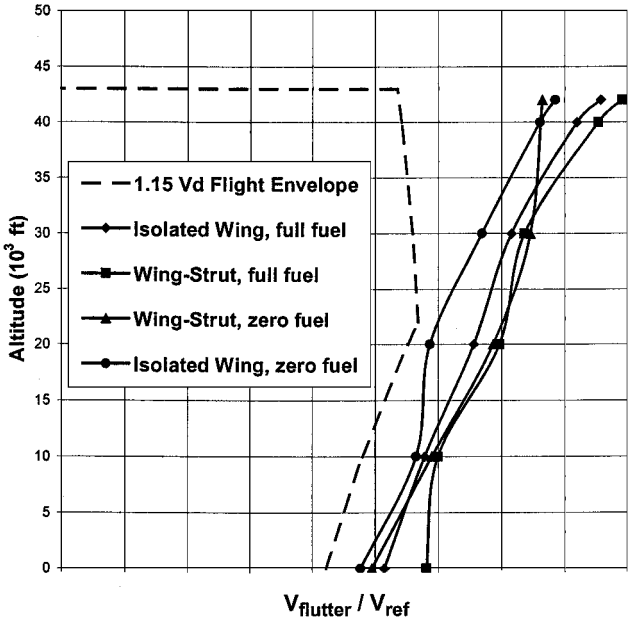

Fig. 8 Flutter boundary vs altitude for different flight conditions of the fuselage-mounted SBW configuration.

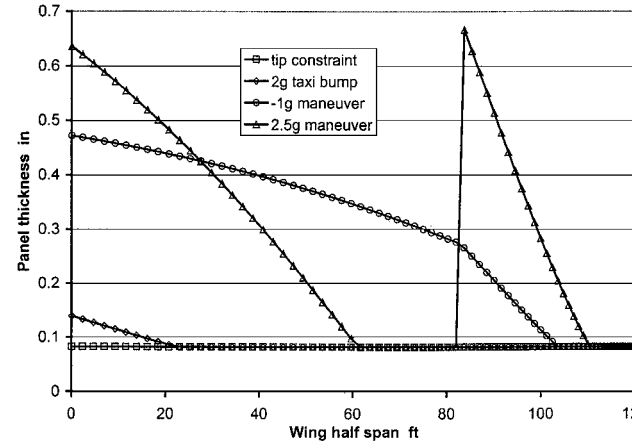

Fig. 9 Panel thickness distributions for the different load cases (fuselage-mounted engine SBW configuration).

structural model is equivalent to the one used for the wing bending weight calculations. The fuel load is distributed into 47 mass elements. For unsteady aerodynamics, the doublet lattice method with compressibility correction for subsonic flight is employed. Aerodynamic loads are simulated using 300 box elements.

To calculate the flutter speed, 10 structural vibration modes are considered. Figure 8 shows the flutter boundary obtained using the PK method in terms of the true air speed. At each altitude, flutter is related to the fundamental wing bending and torsional modes. However, at 30,000 ft, flutter occurs due to coupling of the yawing mode with the first torsional mode. Although not considered here, future aeroelastic studies should be corrected using a more accurate transonic unsteady aerodynamics modeling to simulate the transonic dip effect.

Weights

The aircraft weight is calculated by incorporating several different methods. The majority of the weight equations come from FLOPS.[16] Many of the FLOPS equations were replaced with equations suggested by LMAS. The LMAS and original FLOPS methods do not have the option to analyze the SBW with the desired fidelity. Therefore, the bending material weight from the FLOPS equations is replaced by the bending material weight obtained from the piecewise linear wing load model described earlier.

The wing bending weight is calculated from the piecewise linear beam model, using the averaged panel thickness results of the hexagonal wing–box cross sections for the different load cases (Fig. 9). The overall panel thickness distribution of the wing is obtained by taking the highest value of the panel thickness or cross section at each spanwise position for the different load cases (envelope). To

account for abrupt changes in the material distribution, an additional 1% weight penalty is applied.

The wing weight module to the MDO code was validated using the 747-100 wing.[17] The obtained results show good agreement with the actual 747-100 and with the results obtained from FLOPS[16] and from Torenbeek.[18]

The total weights for the different components (strut, offset, wing) are calculated using the FLOPS equations. Optionally, the wing bending material and strut tension weights are being multiplied by a technology factor to account for the weight reduction achieved by the employment of composite materials by the year 2010.

After computation of the load carrying weights, a 10% nonoptimum factor is applied to account for manufacturing constraints. The total wing weight is calculated from the total load-carrying weight, that is wing, strut, and offset, using the FLOPS equations. The total weights of the different components are determined according to the ratio of their contributions to the load-carrying weight.

LMAS provided a weight estimate of 500 lb for the telescoping sleeve/damper mechanism based on landing gear component data. Weights calculated in the Virginia Polytechnic Institute and State University transport optimization code are identical to FLOPS with the exception of nacelle, thrust reverser, passenger service, landing gear, wing, fuselage, and tail weights, which are calculated from proprietary LMAS formulas. Weight technology factors are applied to major structural components and systems to reflect weight savings due to advances in technology levels from composite materials, advanced electronics, and other technologies described earlier.

Stability and Control

The horizontal and vertical tail areas are first calculated via a tail volume coefficient sizing method. The tail volume coefficients were determined based on Lockheed statistical data. A vertical tail sizing routine was developed to account for the one engine inoperative condition.[8] The engine-out constraint is met by constraining the maximum available yawing moment coefficient to be greater than the required yawing moment coefficient. As specified by FAR requirements, the aircraft must be capable of maintaining straight flight at 1.2 times the stalling speed with the operable engine at its maximum available thrust. The lateral force of the vertical tail provides most of the yawing moment required to maintain straight flight after an engine failure.[11]

The maximum available yawing moment coefficient is calculated at an equilibrium flight condition with a given bank angle and a given maximum rudder deflection.[19] FAR 25.149 limits the maximum bank angle to 5 deg, with some sideslip angle allowed. The stability and control derivatives are calculated using empirical methods of DATCOM as modified by Grasmeyer.[8,20] To allow a 5-deg aileron deflection margin for maneuvering, the calculated deflection must be less than 20–25 deg. The calculated available yawing moment coefficient is constrained in the optimization problem to be greater than the required yawing moment coefficient. If the yawing moment constraint is violated, a vertical tail area scaling factor is applied by the optimizer.

Propulsion

A General Electric GE-90 class high-bypass ratio turbofan engine is used for this design study. An engine deck was obtained from LMAS, and appropriate curves for specific fuel consumption and maximum thrust as a function of altitude and Mach number were found through regression analysis. The general forms of the equations are identical to those found by Mattingly et al.[21] for high-bypass ratio turbofan engines, with coefficients and exponents modified according to LMAS input.

The engine size is determined by the maximum thrust required to meet several constraints. These constraints are thrust at average cruise altitude, available rate of climb at initial cruise altitude, balanced field length, second segment climb gradient, and missed approach climb gradient. The dimensions of the engine nacelles vary with the square root of required thrust, whereas the engine weight is assumed to be linearly proportional to the engine thrust. The specific fuel consumption model is independent of engine scale. A specific fuel consumption technology factor is applied to reflect advances in engine technology.

Performance

The range is calculated by the Breguet range equation (see Ref. 11). The L/D ratio, flight velocity, and specific fuel consumption are determined for the average cruising altitude and Mach number. The initial weight is 95.6% of the TOGW to account for fuel burned during climb to the initial cruise altitude. A reserve range of 500 n miles allows for emergency airport re-routing, extra loiter time while waiting for landing clearance at the end of a maximum range mission, and strong headwinds.

Takeoff and landing performances utilize methods found by Roskam and Lan.[22] The field performance subroutine calculates the second segment climb gradient, balanced field length, missed approach climb gradient, and the landing distance. All calculations are done for hot-day conditions at sea level. Sample drag polars for the aircraft at takeoff and landing were provided by LMAS.[11] Trends are the same for both SBW and cantilever configurations. The actual drag polars use correction factors based on total aircraft wetted area and wing aspect ratio. The second segment climb gradient is the ratio of rate of climb to the forward velocity at full throttle while one engine is inoperative and the gear is retracted.

Roskam and Lan methods are also used to determine the landing distance.[22] Three legs are defined: the air distance from clearing the 50-ft object to the point of wheel touchdown including the flare distance, the free roll distance between touch down and application of brakes, and the distance covered while braking. The lift coefficient on landing approach is the minimum C_L associated with either $V = 1.3V_{\text{stall}}$ or the C_L to meet the tail scrape requirement. The drag coefficient is calculated with gear down.

The missed approach climb gradient is calculated in the same way as the second segment climb gradient with a few exceptions. First, the weight of the aircraft at landing is assumed to be 73% of the TOGW as specified by LMAS. Second, all engines are operational. Third, a landing drag polar distinct from the takeoff drag polar is used. In the present study, the FAR minimum missed approach climb gradient constraint is never violated.

Optimization Results

Choice of the Comparison Baseline

Concerns about the viability of comparing the high wing, fuselage-mounted engine SBW to a low, cantilever wing baseline aircraft lead to a comprehensive assessment of different possible baseline configurations. Main issues were the identification and elimination of the influence of several design specific differences like landing gear stowage for high and low wing configurations, tail sizing for T-tail designs, and fuselage reinforcements for a fuselage-mounted engine aircraft. As a result, to make direct comparisons with the SBW optimum design, three different cantilever aircraft configurations were considered: 1) a low cantilever wing, underwing-mounted engines configuration (Fig. 10), 2) a low cantilever wing, fuselage-mounted engines T-tail configuration, and 3) a

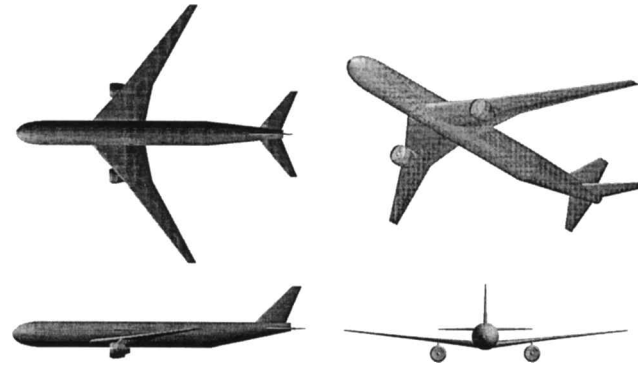

Fig. 10 Conventional cantilever wing configuration with wing-mounted engines.

Table 2 Comparison of the different cantilever aircraft considered as baseline configurations

Parameters	Low wing, wing-mounted engines	Low wing, fuselage-mounted engines	High wing, fuselage-mounted engines
Design variables			
Wing span, ft	217.4	218.4	208.4
Wing $\Lambda_{1/4}$, deg	36.5	36.6	33.9
Wing centerline chord, ft	52.0	52.0	35.2
Wing break chord, ft	24.0	24.0	24.3
Wing tip chord, ft	7.16	7.14	5.78
Wing average, t/c	0.115	0.115	0.116
Maximum engine thrust, lb	70,346	69,945	71,416
Aircraft properties			
TOGW, lb	539,895	539,921	539,550
Wing weight, lb	63,274	64,249	64,763
Fuel weight, lb	187,359	184,411	181,904
Fuselage weight, lb	64,914	66,630	69,859
Wing area, ft^2	4,461.2	4,488.0	4,272.8
Aspect ratio	10.6	10.6	10.2
T/W ratio	0.261	0.260	0.265
Wing loading, lb/ft^2	121	120	126.3
Cruise L/D ratio	23.2	23.7	24.1

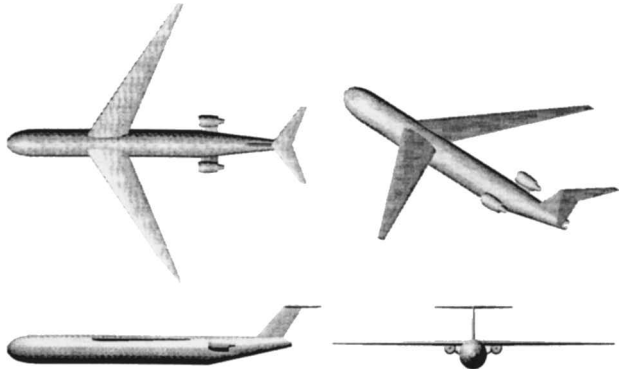

Fig. 11 Conventional cantilever wing T-tail configuration with fuselage-mounted engines.

high cantilever wing, fuselage-mounted engines T-tail configuration (Fig. 11).

Differences in wing geometry for the low and high wing configurations exist. The low wing configuration has a minimum root chord of 52 ft to provide room for wing-mounted landing gear and kick spar. The high wing configuration, without a need for double taper, has fuselage-mounted landing gears, and its chord is linearly interpolated from root to tip. The most significant impact caused by moving the engines from under the wings to the fuselage is the loss of bending moment relief on the wings. Therefore, a slight wing weight increase of the fuselage-mounted engine configurations over the underwing-mounted engines design is observed.

Table 2 shows the minimum TOGW optimization results for the three different cantilever configurations. Overall, there are only slight differences between the three configurations. As expected, the wing weight for the fuselage-mounted engine configurations is higher than for the underwing-mounted engines aircraft. However, this additional weight is not significant enough to have an adverse effect on the TOGW. The high wing configuration is lighter than the low wing configuration, partly due to the absence of the 52-ft root chord constraint.

Previous SBW studies used the low wing, underwing-mounted engines cantilever aircraft as a comparison baseline.[7–9,11] However, for the present study, the high wing, fuselage-mounted engines T-tail cantilever configuration was chosen as a baseline because it is the most similar one to the investigated SBW design (Fig. 12). In essence, this baseline is the SBW configuration without the strut. Note that in the analysis of the high wing configuration, weight and drag penalties due to the fuselage-mounted landing gear bulge were not taken into account. However, this is not expected to have a significant effect on the relative weight differences between the cantilever baseline and the SBW optimum design because this detail applies to both aircraft.

Table 3 Parametric properties of aircraft designs for minimum TOGW and for minimum fuel weight

	Minimum TOGW		Minimum fuel weight	
Properties	Cantilever wing	SBW	Cantilever wing	SBW
Design variables				
Wing span, ft	208.4	220.8	250.7	262.5
Wing $\Lambda_{1/4}$, deg	33.9	31.0	33.0	29.5
Strut $\Lambda_{1/4}$, deg	N/A	23.0	N/A	23.8
Wing average chord, ft	20.5	18.8	20.1	17.0
Wing average, t/c	0.116	0.091	0.106	0.088
Strut chord, ft	N/A	6.73	N/A	6.89
Maximum engine thrust, lb	71,416	60,206	64,923	60,052
Strut position (% of wing half-span)	N/A	70.1	N/A	0.67
Average cruise altitude, ft	38,483	41,933	41,700	43,794
Aircraft properties				
TOGW, lb	539,550	489,379	561,948	512,892
Wing weight, lb	64,763	57,995	98,481	88,870
Fuel weight, lb	181,904	160,499	170,193	149,370
Wing Area, ft^2	4,272.8	4,140.5	5,047.5	4,466.2
Aspect ratio	10.2	11.8	12.5	15.4
T/W ratio	0.265	0.246	0.231	0.234
Wing loading, lb/ft^2	126.3	118.2	111.3	114.8
Cruise L/D ratio	24.1	25.1	28.0	29.5
Improvements				
% TOGW improvement		9.3		8.7
% Fuel improvement		11.8		12.2
% Thrust reduction		15.7		7.5
Important constraints				
Maximum cruise section C_l limit	Active	Active	Active	Active
Second segment climb	Active	Active	Active	
Balanced field length	Active	Active	Active	Active
Initial cruise rate of climb				Active

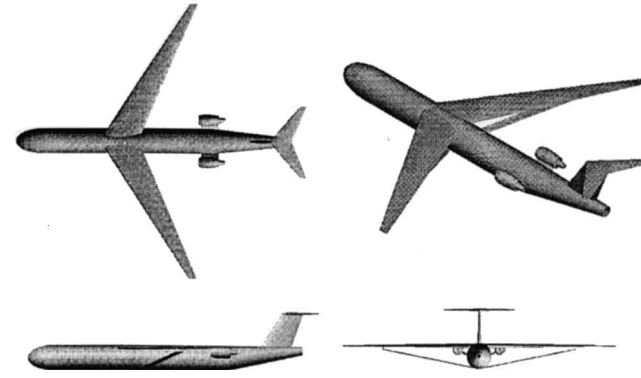

Fig. 12 SBW T-tail design with fuselage-mounted engines.

Mimimum TOGW and Minimum Fuel Consumption

Table 3 shows the parametric results for TOGW minimization and for minimum fuel weight. A comparison of the cantilever and SBW designs shows that, in general, the SBW aircraft have lower wing area, higher aspect ratio, and a reduced wing sweep compared to their cantilever counterparts.

Fuel burn is likely to become an increasingly important factor in aircraft design because the cost of aviation fuel will rise. Any reduction in fuel consumption will be welcome if the fuel price becomes a larger part of transport life cycle cost. Strict emissions regulations will further limit the amount of pollutant discharge permitted by an aircraft. Beyond engine design, reducing the overall amount of fuel consumed for a given flight profile by improved configuration design will also reduce the total amount of emissions.

Minimum TOGW Versus Minimum Fuel Consumption

For minimum TOGW and minimum fuel cases, the SBW is superior for the selected objective functions. Whereas the SBW has an 9.3% decrease in TOGW, the savings in fuel consumption are even more impressive. A SBW has a 11.8% lower fuel burn than a cantilever configuration when optimized for minimum TOGW and a 12.2% lower fuel weight when both are optimized for minimum fuel weight.

The minimum fuel SBW has a higher wingspan to increase the L/D and flies at higher altitudes. The TOGW of the minimum fuel SBW is 8.7% lower than an equivalent cantilever design and 4.8% higher than a minimum TOGW SBW. The SBW L/D increases from 25.1 to 29.5 going from the minimum TOGW to the minimum fuel case and from 24.1 to 28.0 for the cantilever configuration. This improved aerodynamic efficiency is achieved by increasing the wing span, coming at the expense of an increased structural weight.

Airport noise pollution can limit the types of aircraft permitted to use certain urban airfields and impose operational restrictions on those that do. Minimizing engine size can also be expected to reduce the noise generated if the engine is of similar design. Minimum TOGW SBW engine thrust is reduced by 15.7% over the equivalent cantilever design, probably reducing airport noise pollution by a similar amount.

General Observations

One of the main concerns for a high aspect ratio design that satisfies a long-range mission is the available fuel volume in the wings. For low wing commercial airplane designs, fuel is carried in the wing center section under the passenger floor. On military high wing airplanes, some fuel can be carried above the cargo compartment. However, for a commercial high wing aircraft, the safety issues associated with carrying fuel above the passenger compartment far outweigh its practicality. In this study, the fuel volume constraint ensures that the there is enough fuel volume in the wing tanks to store the required fuel to complete the mission profile. In all of the optimized designs, it was found that the fuel volume constraint was inactive, indicating that there is more than enough volume in the wing tanks for the required amount of fuel. A detailed description of the fuel volume calculation may be found in Ref. 7.

Several issues concerning the SBW design have not been addressed in this study but might warrant further investigation. The first one is that high aspect ratio wings are more susceptible to aileron reversal. Because one of the strengths of the SBW design lies in its high aspect ratio wings, this detail should be pursued in future studies. Also, an additional constraint for engine-out at cruise altitude should be added. For twin-engine airplanes, this constraint requires that, at a specified altitude, the airplane should be able to cruise with one engine inoperable. Another issue that has been raised with the designs in this study is longitudinal instabilities, known as the pitch-up problem associated with high aspect ratio swept wings. This phenomenon is related to the deep stall problem of fuselage-mounted engine T-tail designs. Because of the exploratory nature of this study, none of these issues have been addressed herein. However, the mentioned problems apply to both the cantilever baseline and the SBW design. Therefore, they should not affect the presented relative benefits of the SBW concept.

In this study, only optimization results were presented. This provides a point solution without any indication of the design sensitivities with respect to the constraints. To better understand the MDO process in the design of the SBW aircraft, a study on the effects of the constraints on the designs has been conducted. This includes thumbprint plots of T/W vs W/S, which have been traditionally used by preliminary airplane designers to study aircraft design concepts. A detailed discussion of these aspects can be found in Ref. 23.

Conclusions

Virginia Polytechnic Institute and State University transport studies have shown the potential of the SBW over traditional cantilever configurations. After much added realism by a major airframe manufacturer, in the form of weight penalties for the SBW, the MDO analysis shows that the SBW demonstrates major improvements over the cantilever wing configuration. A significant reduction in TOGW was found, but the greatest benefit of the SBW is a reduced fuel consumption and smaller engine size. These results indicate that the SBW will cost less, limit pollutant discharge, and reduce noise pollution for urban airports.

The special design of the SBW required the development of a wing sizing module suitable to fully exploit the benefits of this structural configuration. After validation with existing aircraft like the 747-100, the module was used for wing sizing and structural weight computation of the SBW. Consideration of the actual in-flight maneuver loads not only increases the accuracy in wing sizing but also gives the potential for further weight savings. This is especially important within a multidisciplinary design environment where, due to synergistic interaction, even small weight savings in one component are very likely to result in further weight reductions for other components.

Acknowledgments

This project was funded by NASA Langley Research Grant NAG 1-1852. Part of the work was done under subcontract from Lockheed Martin Aeronautical Systems in Marietta, Georgia, who also provided valuable contributions in data, design methods, and advice. The authors would like to thank their coworkers Bernard Grossman (multidisciplinary design optimization, response surface methodology, computational fluid dynamics (CFD)), Joseph A. Schetz (computaton of the interference drag, innovative design concepts), William H. Mason (airplane design issues and multidisciplinary design optimization), and Philippe-Andre Tetrault (CFD-based response surface for the interference drag). Without their valuable discussions and contributions to this work, both the quality and the quantity of the presented results would have been significantly lower.

References

[1]Pfenninger, W., "Design Considerations of Large Subsonic Long Range Transport Airplanes with Low Drag Boundary Layer Suction," Northrop Aircraft, Inc., Rept. NAI-54-800 (BLC-67), Nov. 1954.

[2]Gunston, B., *Giants of the Sky: The Biggest Aeroplanes of all Time*, Patrick Stephens, Wellingborough, England, U.K., pp. 240–250.

[3]Kulfan, R. M., and Vachal, J. D., "Wing Planform Geometry Effects on Large Subsonic Military Transport Airplanes," Boeing Commercial Airplane Co., Air Force Flight Dynamics Lab. Rept. AFFDL-TR-78-16, Feb. 1978.

[4]Jobe, C. E., Kulfan, R. M., and Vachal, J. D., "Wing Planforms for Large Military Transports," AIAA Paper 78-1470, Aug. 1978.

[5]Turriziani, R. V., Lovell, W. A., Martin, G. L., Price, J. E., Swanson, E. E., and Washburn, G. F., "Preliminary Design Characteristics of a Subsonic Business Jet Consept Employing an Aspect Ratio 25 Strut-Braced Wing," NASA CR-159361, Oct. 1980.

[6]Smith, P. M., DeYoung, J., Lovell, W. A., Price, J. E., and Washburn, G. F., "A Study of High-Altitude Manned Research Aircraft Employing Strut-Braced Wings of High-Aspect Ratio," NASA CR-159262, Feb. 1981.

[7]Grasmeyer, J. M., Naghshineh-Pour, A., Tetrault, P.-A., Grossman, B., Haftka, R. T., Kapania, R. K., Mason, W. H., and Schetz, J. A., "Multidisciplinary Design Optimization of a Strut-Braced Wing Aircraft with Tip-Mounted Engines," Multidisciplinary Analysis and Design Center for Advanced Vehicles, MAD Rept. 98-01-01, Virginia Polytechnic Inst. and State Univ., Blacksburg, VA, 1998.

[8]Grasmeyer, J. M., "Multidisciplinary Design Optimization of a Strut-Braced Wing Aircraft," M.S. Thesis, Dept. of Aerospace and Ocean Engineering, Virginia Polytechnic Inst. and State Univ., Blacksburg, VA, April 1998.

[9]Martin, K. C., and Kopec, B. A., "A Structural and Aerodynamic Investigation of a Strut-Braced Wing Transport Aircraft Concept," NAS1-96014, Nov. 1998.

[10]*DOT User's Manual, Ver. 4.20*, Vanderplaats Research and Development, Inc., Colorado Springs, CO, 1995.

[11]Gundlach, J. F., Tetrault, P.-A., Gern, F. H., Nagshineh-Pour, A. H., Ko, A., Schetz, J. A., Mason, W. H., Kapania, R. K., Grossman, B., and Haftka, R. T., "Conceptual Design Studies of a Strut-Braced Wing Transonic Transport," *Journal of Aircraft*, Vol. 37, No. 6, 2000, pp. 976–983.

[12]Hoerner, S. F., *Fluid Dynamic Drag: Practical Information on Aerodynamic Drag and Hydrodynamic Resistance*, Hoerner Fluid Dynamics, Bakersfield, CA, 1965.

[13]Pirzadeh, S., "Structured Background Grids for Generation of Unstructured Grids by Advancing-Front Method," *AIAA Journal*, Vol. 31, No. 2, 1993, pp. 257–265.

[14]Frink, N. T., Pirzadeh, S., and Parikh, P., "An Unstructured-Grid Software System for Solving Complex Aerodynamic Problems," NASA CP-3291, May 1995.

[15]Frink, N. T., Parikh, P., and Pirzadeh, S., "A Fast Upwind Solver for the Euler Equations on Three-Dimensional Unstructured Meshes," AIAA Paper 91-0102, Jan. 1991.

[16]McCullers, L. A., *FLOPS Flight Optimization System*, Release 5.94, User's Guide, NASA Langley Research Center, Hampton, VA, Jan. 1998.

[17]Gern, F. H., Sulaeman, E., Naghshineh-Pour, A., Kapania, R. K., and Haftka, R. T., "Structural Wing Sizing for Multidisciplinary Design Optimization of a Strut-Braced Wing," *Journal of Aircraft*, Vol. 38, No. 1, 2001, pp. 154–163.

[18]Torenbeek, E., "Development and Application of a Comprehensive, Design Sensitive Weight Prediction Method for Wing Structures of Transport Category Aircraft," Delft Univ. of Technology, Rept. LR-693, Delft, The Netherlands, Sept. 1992.

[19]Roskam, J., "Methods for Estimating Stability and Control Derivatives of Conventional Subsonic Airplanes," Roskam Aviation and Engineering Corp., Lawrence, KS, 1971.

[20]Grasmeyer, J. M., "Stability and Control Derivative Estimation and Engine-Out Analysis," Rept. VPI-AOE-254, Virginia Polytechnic Inst. and State Univ., Blacksburg, VA, Jan. 1998.

[21]Mattingly, J. D., Heiser, W. H., and Daley, D. H., *Aircraft Engine Design*, AIAA, Washington, DC, 1987, p. 36.

[22]Roskam, J., and Lan, C.-T. E., Airplane Aerodynamics and Performance, DARCorporation, Lawrence, KS, 1997.

[23]Ko, A., Grossman, B., Mason, W. H., Haftka, R. T., "The Role of Constraints in the MDO of a Cantilever and Strut-Braced Wing Transonic Commercial Transport Aircraft," Society of Automotive Engineers, SAE Paper 2000-01-5609, Oct. 2000.